# Experimental study of ac Josephson effect in gate-tunable $(Bi_{1-x}Sb_x)_2Te_3$ thin-film Josephson junctions

Yuusuke Takeshige, Sadashige Matsuo, Tokyo, 113-8654, Japan

Sadashige Matsuo, Sadashige Matsuo, Sadashige Matsuo, Sadashige, And Sadashige, Sadashige,

(Received 7 December 2019; accepted 20 February 2020; published 11 March 2020)

We report on measurements of the ac Josephson effect in three-dimensional topological insulator (TI) Josephson junctions with Fermi energy tuning using a back gate. We successfully tune the Fermi energy into the bulk gap of the TI. We observe that the Josephson energy as a function of the gate voltage has a dip feature, indicating the presence of specular Andreev reflections. We study the ac Josephson effect with detection of both Shapiro steps and Josephson emission. The obtained results show no signature of Majorana modes. With the support of simulations, we conclude that the observation of the fractional ac Josephson effect may be complicated by both a large parallel capacitance and a small ratio of current carried in  $4\pi$  period modes compared to conventional  $2\pi$  modes.

DOI: 10.1103/PhysRevB.101.115410

### I. INTRODUCTION

Majorana fermions (MFs) were discovered as one of the solutions to the Dirac equation [1]. After several decades, Kitaev proposed that MFs can appear at the edge of a spinless onedimensional superconductor [2]. This proposal has promoted research of the MFs in condensed-matter physics, especially in order to reveal the non-Abelian statistics and possible application to topological quantum computation [3–5]. One of the platforms for generating MFs is to engineer topological superconductivity [2] in hybrid superconducting systems. Superconducting junctions such as junctions of semiconductor nanowires [6,7] and topological insulators (TIs) [8,9] have been proposed theoretically. Experimentally, signatures of MFs such as localized zero-energy modes [10-12], exponential protection of the localized modes [13], and  $4\pi$  periodic Josephson supercurrent [14–21] have been observed. In addition to the junctions mentioned above, ferromagnetic atoms on superconductors have also shown the localized zeroenergy modes [22,23], and superconducting junctions of Dirac semimetals have also shown evidence of the  $4\pi$  periodic Josephson supercurrent [24,25].

In superconducting junctions of semiconductor nanowires or ferromagnetic atoms, a strong magnetic field or ferromagnetism are required for most cases of engineering of MFs, resulting in a soft superconducting gap that degrades topological protection of MFs. However, the TI-superconductor junctions do not need such a strong magnetic field or ferromagnetism.

We note that the weak magnetic fields are still required to induce the vortices holding the localized MFs in the systems [26,27]. For the two-dimensional TI Josephson junction (JJ), the ac Josephson effect has been studied with Fermi energy tuning [16,17]. On the contrary, all the previous reports on the ac Josephson effect of three-dimensional (3D) TI JJs do not address Fermi energy tuning [15,18–20], meaning that the bulk contributions may remain. Therefore, it is important to demonstrate that the surface states are essential for observations of a fractional ac Josephson effect that indicates Majorana modes. Furthermore, routes toward electrical control and braiding of MFs in 3D TI-based systems have been proposed [27,28] allowing MFs engineered in superconducting junctions of 3D TI to be utilized for demonstration of the non-Abelian statistics. This is the additional motivation to study 3D TI JJs.

Here we show experimental results of JJs with weak links formed from gate-tunable  $(Bi_{1-x}Sb_x)_2Te_3$  (BST) thin films. We succeed in electrical control of normal resistance  $(R_n)$  and switching current  $(I_{sw})$  of the JJs. We find that the observed  $I_{sw}R_n$  shows a dip feature near the charge neutral point assigned to the analog of specular Andreev reflection. We measure the Shapiro steps of the JJ and observe that both odd and even integer-multiple Shapiro steps appear even around the charge neutral point with no evidence of the fractional ac Josephson effect. Additionally, we measured Josephson emission and detect conventional spectra, which is also contrary to the prediction for junctions with Majorana modes. We discuss possible reasons why the measured ac Josephson effect is conventional.

We choose BST as a 3D TI because the topological nature has already been demonstrated by angle-resolved

<sup>\*</sup>sadashige.matsuo@riken.jp

<sup>†</sup>tarucha@riken.jp

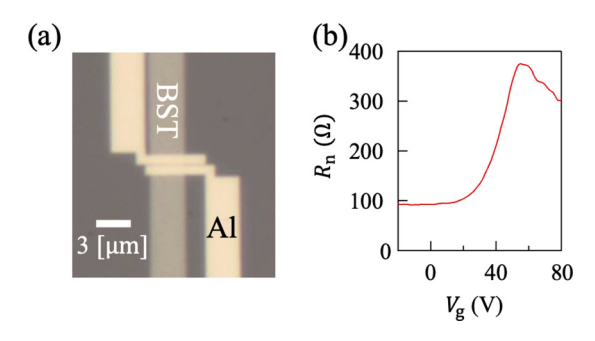


FIG. 1. (a) The top view of sample A. (b) The  $V_g$  dependence of  $R_n$ .  $R_n$  is defined as an average of differential resistance obtained at I larger than  $I_{sw}$ .

photoemission spectroscopy (ARPES) measurements [29], and also the features of Dirac electrons on the surface have been reported in electron transport experiments of, for example, Shubnikov–de Haas oscillations [30] and the quantum Hall effects [31]. In addition, the Fermi energy of BST can be tuned by chemical doping and also electric-field tuning. We use a thin film of  $(Bi_{1-x}Sb_x)_2Te_3$  (x=0.8) grown on heattreated SrTiO<sub>3</sub> substrate (111) by molecular beam epitaxy. The thickness of  $(Bi_{1-x}Sb_x)_2Te_3$  is eight quintuple layers (8 nm) and the out-of plane direction is (111). This is thick enough to avoid the hybridization of the top and bottom surface states [29]. The SrTiO<sub>3</sub> substrate is 0.5 mm thick. We can tune the Fermi energy electrically by applying gate voltage on the back of the substrate.

We fabricated these BST films into JJs devices. The mesas were patterned by Ar ion etching, and superconducting contacts were fabricated with conventional electron beam lithography and metal deposition. Before the metal deposition, we dipped the sample in diluted HCl to remove the oxidized surface layer [32]. Next, we deposited Ti(0.5 nm)/Al(30 nm) for sample A and MoRe (80 nm) for sample B, respectively. An optical image of sample A is shown in Fig. 1(a). Electrical measurements were carried out in a dilution refrigerator with a base temperature of 30 mK. We executed four-terminal measurements with dc current bias.

### II. EXPERIMENTAL RESULTS

First, we focus on the gate voltage  $(V_g)$  dependence of  $R_n$  of sample A. Figure 1(b) shows the  $R_n-V_g$  plot. A peak of  $R_n$  can be seen at  $V_g\approx 55$  V, indicating the charge neutral point. Next the  $V_g$  dependence in the superconducting region is studied. Figure 2(a) shows the differential resistance as a function of  $V_g$  and current (I) for sample A. The zero-resistance region around bias current I=0 nA indicates that the supercurrent flows through the JJ. The sharp dV/dI peak (white lines) when the current increases indicates the switching of the junction from super (black) to normal (blue) branches. Here V is the measured voltage. We define the switching current  $I_{\rm SW}$  as I at the sharp peak with I>0. Since  $I_{\rm SW}$  depends strongly on  $V_g$  and  $R_n$ , it is concluded that the supercurrent can be controlled by the gate voltage. This guarantees that the supercurrent flows through the BST film.

Figure 2(b) shows the dV/dI as a function of I and a magnetic field B perpendicular to the film at  $V_g = 0$  V. The

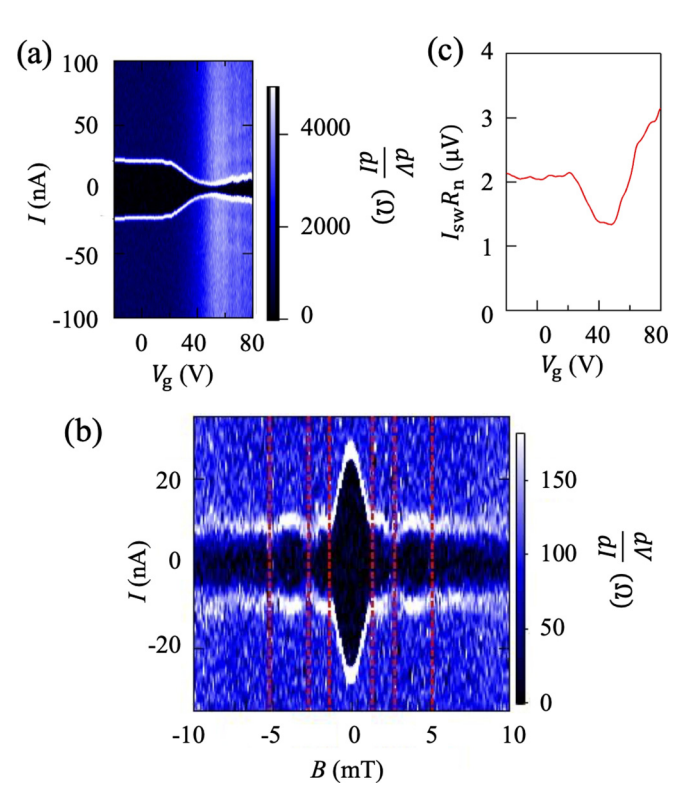


FIG. 2.  $V_{\rm g}$  and I dependence of differential resistance (a). (b) Bias current and the magnetic field dependence of differential resistance. Red dashed lines indicate the nodes' positions of the Fraunhofer pattern. (c)  $V_{\rm g}$  dependence of  $I_{\rm sw}R_{\rm n}$ ; a dip feature appears near the charge neutral point.

B dependence of  $I_{sw}$  approximately follows the Fraunhofer pattern, which is usually observed in conventional planar JJ devices. This result also supports that the supercurrent flows through the BST films. However, there are two unexpected features found in the magnetic field dependence. First, the intervals between nodes as indicated by the red dashed lines are not constant. Second,  $I_{sw}$  does not become 0, even at the node point. These features can indicate a nonuniform supercurrent distribution because the magnetic field dependence can take the shape of a sum of Fraunhofer patterns having different periods. In this case, the intervals cannot be constant and a finite supercurrent can remain even at the nodes. The junction area calculated from the junction geometry is  $0.3 \,\mu\text{m}^2$ , which is inconsistent with the area of  $0.81 \,\mu\text{m}^2$  evaluated from the distance between the second and third nodes. A similar inconsistency has been previously assigned to the flux-focusing effect [33,34].

We now provide further discussion on the  $V_{\rm g}$  dependence in terms of the Josephson energy. From the result of Fig. 2(a), we calculate the product  $I_{\rm sw}R_{\rm n}$  at each  $V_{\rm g}$  as shown in Fig. 2(c). The value of  $I_{\rm sw}R_{\rm n}$  is of the order of a few  $\mu \rm V$ , which is much smaller than the Al superconducting gap  $\simeq 170~\mu \rm V$ , indicating poor transparency of the BST/Al interface. The evaluated  $I_{\rm sw}R_{\rm n}$  has a dip feature around  $V_{\rm g} \simeq 50~\rm V$ . In JJs of other 3D TIs or graphenes, similar dip features have been reported in the gate dependence of  $I_{\rm sw}R_{\rm n}$  [32,35–40]. We attribute this dip to the influence from the electron-hole puddles, the locally distributed p- or n-doped regions that

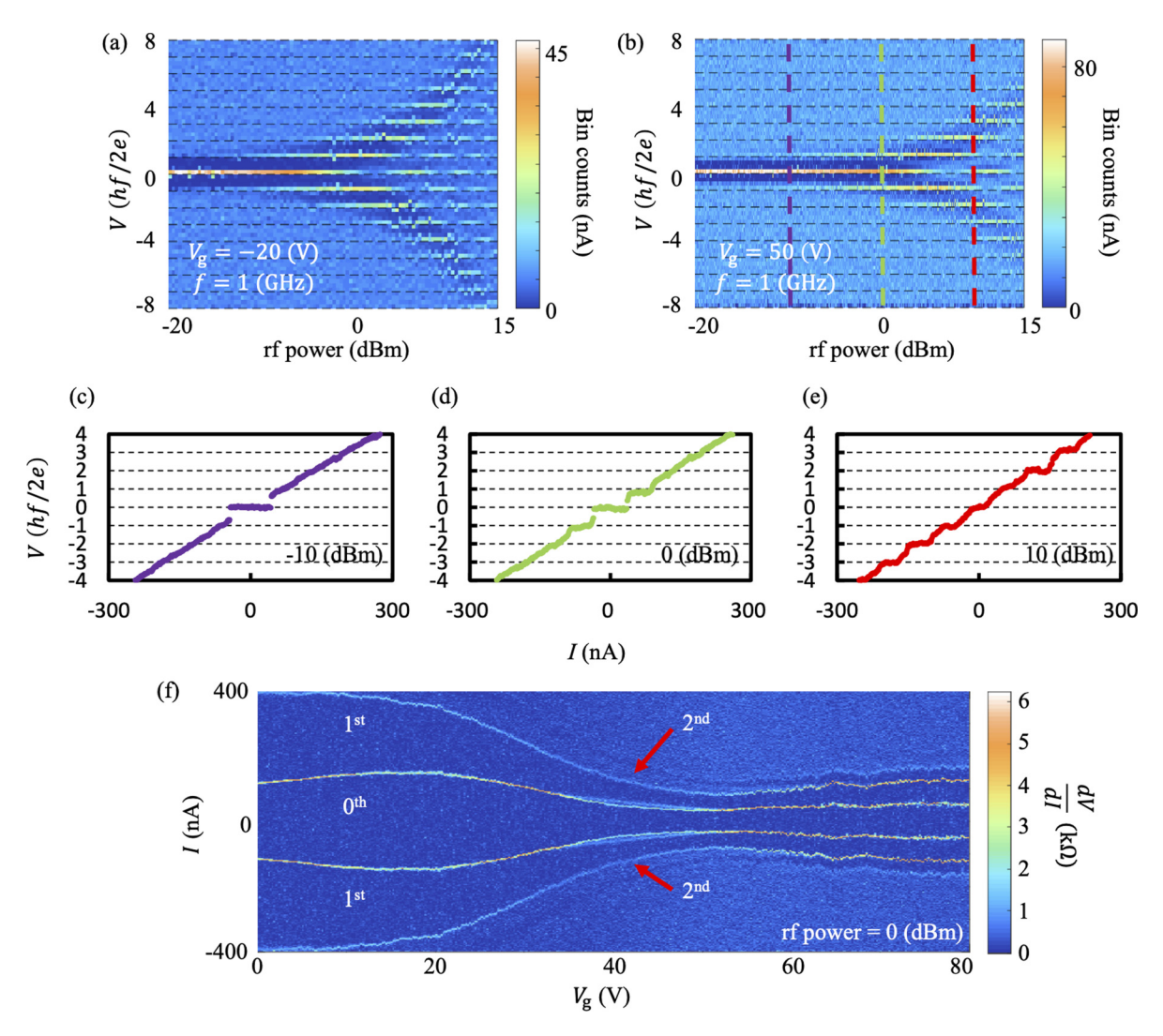


FIG. 3. Shapiro steps of sample A with  $V_{\rm g}=-20\,{\rm V}$  (a) and  $V_{\rm g}=50\,{\rm V}$  (b). In both data sets, the first steps appear clearly. (c)–(e) Shapiro step measurements along each dashed line in (b). The colors of each graph correspond to the colors of the dashed lines in (b). (f)  $V_{\rm g}$  dependence of the Shapiro steps in sample A showing that the first step appears for the full range of gate voltage studied. In all cases, the frequency is 1 GHz.

appear near the charge neutral point due to inhomogeneity. The transport phenomenon related to the puddles has been studied intensively in graphene devices, both theoretically and experimentally [41–45]. The  $I_{sw}$  suppression [45] can be attributed to the charge scattering at the boundaries of electron-hole puddles taking the form of specular Andreev reflections [46]. This specular Andreev reflection does not have the retroreflection property of Andreev events, causing a reduction of  $I_{sw}R_n$  near the charge neutral point [45] compared with that in the carrier-doped regions. The existence of the puddles is observed also in 3D TIs [47] and the specular Andreev reflection is theoretically predicted on the interface of 3D TI and a superconductor [48]. Therefore, the same scenario can work for the  $I_{sw}R_n$  suppression near the charge neutral point as shown in Fig. 2(c). We note that the  $I_{sw}R_n$ reduction can be ascribed to fluctuation [36-39] or ripples [40]. Sample A, however, has small hysteresis [49]. This indicates that the difference between the measured switching current and the critical current does not play an important role in sample A. In addition, our sample is not monolayer,

and therefore it should contain fewer ripples. Finally, we conclude that the observed  $I_{sw}R_n$  dip feature arises from the electron-hole puddles.

We next move to the measurement results of V versus current I while irradiating rf microwave excitation to the JJ. The binning method is used to evaluate the Shapiro steps [15]. Measured dc voltage is converted to the histogram of the voltage for each I in bins of  $0.25 \times hf/2e$ . Here h is Planck's constant, f is the irradiated microwave frequency, and -e is the electron charge. As the source current is swept at a constant rate, the counts per bin reflect the current on a given Shapiro step. Figures 3(a) and 3(b) show the bin counts of the measurement as a function of rf power of the microwave at  $V_{\rm g}=-20$  and 50 V, respectively. The histogram is expected to show peaks originating from the Shapiro steps at quantized voltages of multiples of hf/2e in conventional JJs, and odd number multiples would disappear in topological JJs. In Figs. 3(a) and 3(b), all Shapiro steps including the odd number steps appear clearly. The steps can also be observed in I-V curves of Figs. 3(c)-3(e), which

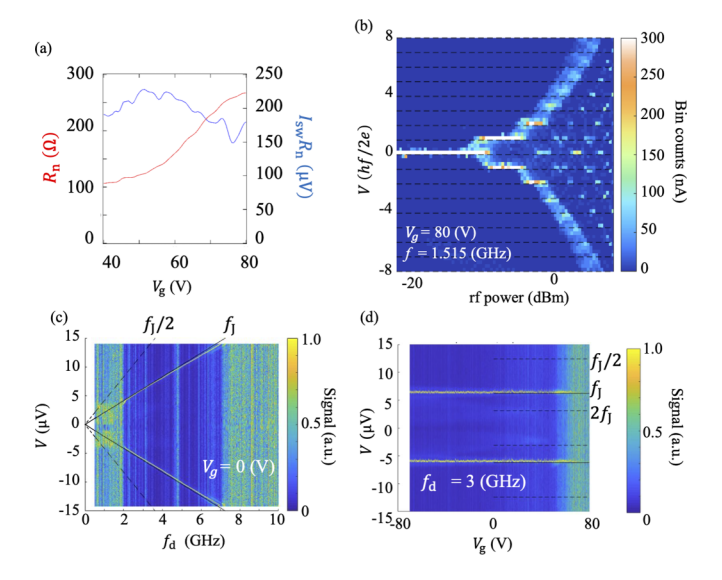


FIG. 4. Measurement of the Josephson effects for sample B: (a)  $V_{\rm g}$  dependence of  $R_{\rm n}$  and  $I_{\rm sw}R_{\rm n}$  of sample B. (b) The Shapiro steps at  $V_{\rm g}=80\,{\rm V}$ . (c) The measured Josephson emission at  $V_{\rm g}=0\,{\rm V}$ . The dark solid line indicates  $f_{\rm J}$  and the dashed line indicates  $f_{\rm J}/2$ . A strong emission feature is only seen at  $f_{\rm J}$  with a weak signature of higher harmonics around  $2f_{\rm J}$ . (d)  $V_{\rm g}$  dependence of Josephson emission. The resonance only occurs when the frequency is  $f_{\rm J}$  and weakly at  $2f_{\rm J}$ . Here the dark solid line is  $f_{\rm J}$  and dashed lines are  $f_{\rm J}/2$  or  $2f_{\rm J}$ .

correspond to the cuts of Fig. 3(b). The colors of the graphs are the same as the colors of the dashed line in Fig. 3(b). Figure 3(f) shows dV/dI as a function of  $V_{\rm g}$  and bias current. The first step appears at all gate voltages. This indicates that the fractional ac Josephson effect is not observed in this JJ.

One possible reason why the odd number Shapiro steps remain is the small  $I_{\rm sw}R_{\rm n}$ . According to previous studies [15,50], in order to observe the vanishing of the odd number Shapiro steps in coexistence of both  $4\pi$  and  $2\pi$  periodic components with dominant  $2\pi$  modes, the microwave frequency should satisfy the condition of

$$f < \left(2eI_{\rm c}^{4\pi}R_{\rm n}\right)/h,\tag{1}$$

Here  $I_{\rm c}^{4\pi}$  is the critical current of the  $4\pi$  periodic component. In our case, assuming the possibility of a low contribution in the supercurrent from the  $4\pi$  periodic modes combined with the small  $I_{\rm sw}R_{\rm n}$ , we consider that the vanishing odd number steps would only be observed for a low-frequency range. Since the Shapiro step signals become weaker as the frequency is lowered, it becomes difficult to measure well-resolved features.

To increase  $I_{\rm sw}R_{\rm n}$ , we use sample B with MoRe as the contact superconductor. MoRe has a larger superconducting gap than Al so that a larger  $I_{\rm sw}R_{\rm n}$  is expected. The measured  $R_{\rm n}$  versus  $V_{\rm g}$  is shown as a red line in Fig. 4(a).  $R_{\rm n}$  increases monotonically with  $V_{\rm g}$  and then starts to saturate around  $V_{\rm g}=80\,{\rm V}$ . This saturation behavior implies that the BST at  $V_{\rm g}=80\,{\rm V}$  is around the charge neutral point. The calculated  $I_{\rm sw}R_{\rm n}$  is around 180  $\mu{\rm V}$  in  $V_{\rm g}=80\,{\rm V}$ , shown as a blue line in Fig. 4(a). This result means that the upper limit described in

Eq. (1) of the MoRe JJs is almost 100 times larger than the Al JJs.

Then we move to the analysis of Shapiro steps. Here the irradiated microwave frequency is f = 1.515 GHz. The result as a function of bias voltage and the rf power is shown in Fig. 4(b). The first step clearly appears.

We also measured the Josephson emissions of sample B in our emission measurement setup [17]. With applying bias voltage V, the intensity of the emitted microwave from the JJ at each detection frequency ( $f_d$ ) is analyzed. Measurements performed at each detection frequency have a background subtraction, taken as the amplitude at zero current, and they are normalized by the peak amplitude at that frequency. Emission features at  $f_J = 2eV/h$  and  $f_J/2 = eV/h$  are expected from conventional and topological JJs, respectively. Figure 4(d) shows the gate voltage dependence of the emitted RF signal at  $f_d = 3$  GHz. The dark solid and dashed lines indicate  $f_J$  and  $f_J/2$  or  $2f_J$ , respectively. Even in this case the observed resonance is seen only in  $f_J$ . The emission signal is observed only at  $f = f_J$  with a weak second-harmonic feature around  $2f_J$  for some gate voltages.

One possible reason why we are unable to observe vanishing odd number Shapiro steps and the appearance of  $f_{\rm J}/2$  emission may be the large parallel capacitance ( $\simeq 100\,{\rm pF}$ ) originating from the huge dielectric constant of SrTiO $_3$  substrate. In fact, prior theoretical research indicates that high junction capacitance can complicate the observation of the missing of Shapiro steps [51]. In addition, we also speculate that a small  $4\pi$  periodic current contribution is preventing the detection of the fractional Josephson effect. We discuss these points based on numerical simulation below.

## III. DISCUSSIONS

The salient features of the ac Josephson effect in a weak link with both  $4\pi$  periodic and  $2\pi$  periodic modes were described by Dominguez *et al.* using a two-periodicity resistively shunted Josephson junction model [50]. More recently, the two-periodicity model has been expanded to more completely capture the behavior of real devices. For example, the effects of Joule heating [18] and capacitance [51] have been investigated. The resistively capacitively shunted junction (RCSJ) model including the two components of  $2\pi$  and  $4\pi$  periodic supercurrent is based on the simple current biased circuit, which is depicted in Fig. 5(a). The time evolution of the phase difference,  $\phi$ , is written as

$$\frac{C}{I_{c}} \frac{\hbar}{2e} \frac{d^{2}\phi}{dt^{2}} + \frac{\hbar}{2e} \frac{1}{RI_{c}} \frac{d\phi}{dt} + \frac{i_{sc}(\phi)}{I_{c}} = \frac{1}{I_{c}} [i_{0} + i_{1} \sin(\omega_{ac}t)],$$
(2)

where  $\hbar$  is Dirac's constant, C is the junction capacitance, R is the resistance including the junction resistance  $R_{\rm JJ}$  and a parallel shunt resistance  $R_{\rm shunt}$ ,  $I_{\rm c}$  is the critical current of the JJ, and  $i_0$  is the external current bias. The variable  $i_{\rm sc}(\phi)$  is the current phase relationship of the entire junction, which is comprised of two components with different periodicity,  $i_{\rm sc}(\phi)=i_{2\pi}\sin(\phi)+i_{4\pi}\sin(\phi/2)$ . Here, we consider the value of  $r=i_{4\pi}/i_{2\pi}$ . We also define the Stewart-McCumber parameter  $\beta_{\rm c}=(2eR^2I_{\rm c}C)/\hbar$ . We assume that  $i_{4\pi}\ll i_{2\pi}$ , because only electrons whose incident angle is perpendicular to

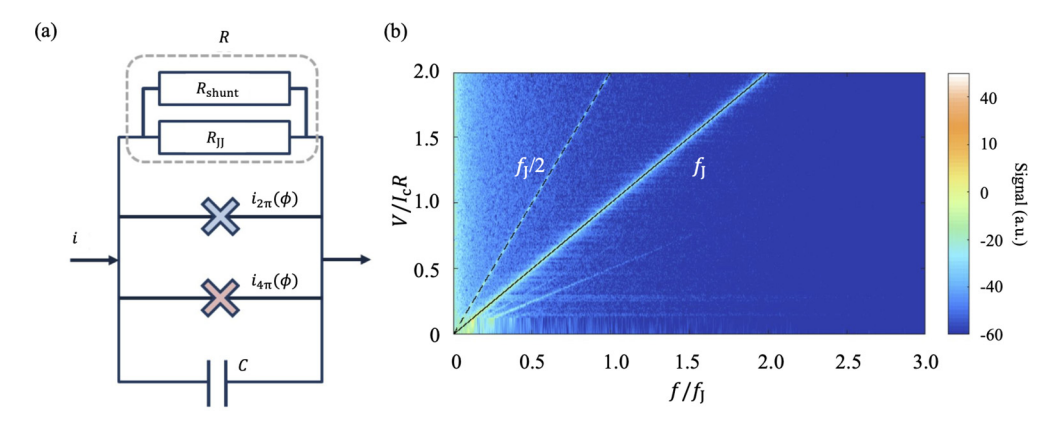


FIG. 5. (a) The circuit diagram of the RCSJ model. (b) Example simulation results for r = 0.15 and  $\beta_c = 10$ . The black line indicates  $f_J$  emission, and the black dashed line indicates  $f_J/2$  emission.

the interface between the superconductors and BST contribute to the  $4\pi$  periodic component [8]. Here we consider only Josephson emission for simplicity. So we focus on the case with no external drive such that  $i_1 = 0$ .

For each set of device parameters, we solve the RCSJ model and perform a fast Fourier transform (FFT) calculation of  $\phi(t)$  traces to extract plots such as that shown in Fig. 5(b). We then extract the amplitude of Josephson emission,  $A_{2\pi}$  and  $A_{4\pi}$  at  $f_J$  and  $f_J/2$ , respectively.

We consider the effects of variation of  $R_{\rm shunt}$ , C, and r in Fig. 6. Since changing  $R_{\rm shunt}$  is equal to changing  $\beta_{\rm c}(\propto C)$ , we focus on the values of  $\beta_{\rm c}$  and r. Figure 6 shows the ratio

of  $A_{2\pi}$  and  $A_{4\pi}$  for different  $\beta_c$  and r. For high frequency, all data sets in Fig. 6(a) collapse to a single line indicating that the ratio of emission amplitudes is determined by the ratio r. We can also see the crossover in the very-low-frequency region  $(f_J \ll 5 \, \text{GHz})$  in which  $A_{4\pi}/A_{2\pi}$  abruptly becomes large and reaches 1. This indicates the crossover from the purely  $4\pi$  regime to the  $4\pi + 2\pi$  regime [52] as the frequency becomes high. In contrast, as capacitance becomes larger (equal to higher  $\beta_c$ ), this crossover becomes lower frequency, as shown in Fig. 6(b). This means that in the high C case, the purely  $4\pi$  periodic region is difficult to access. We also see the effect of r. Lowering r decreases the relative emission amplitudes

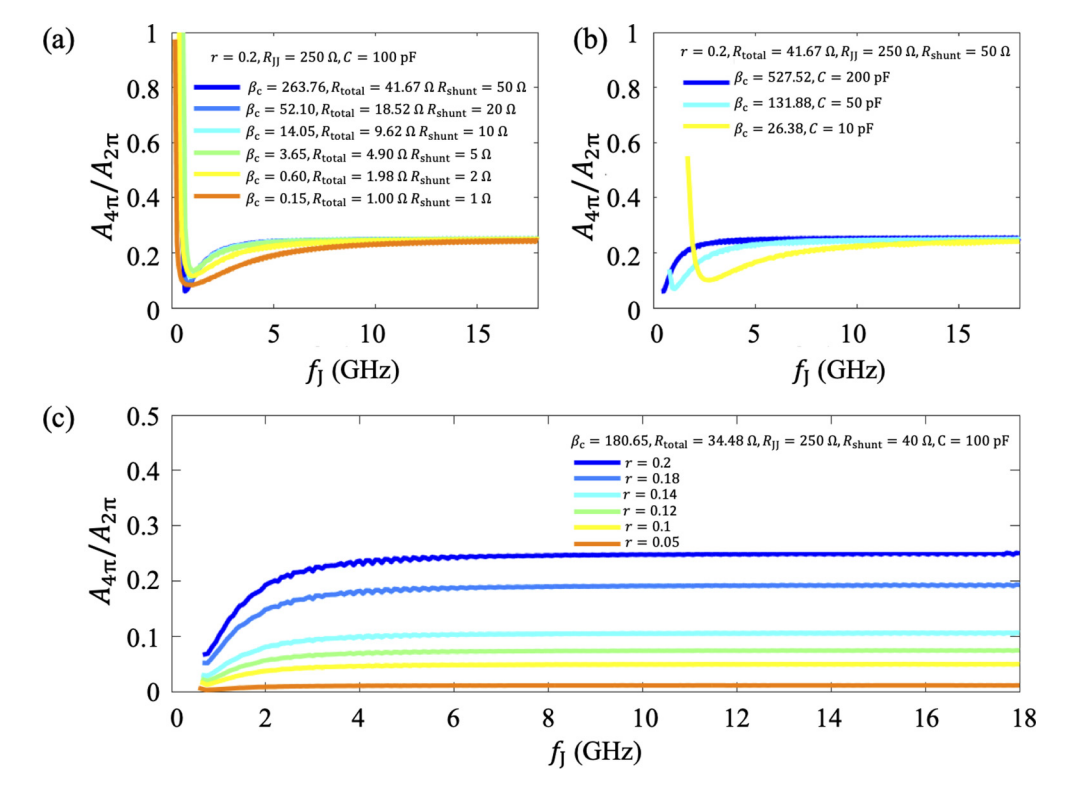


FIG. 6. (a) Simulation results for different  $R_{\text{shunt}}$  with r = 0.2. This is equal to changing  $\beta_c$ .  $A_{4\pi}/A_{2\pi}$  features for high frequency are found to collapse onto a single line with a value related to r. (b) Simulation results for different C. In lower frequency, we can see the crossover regime in which  $f_J/2$  may be enhanced beyond the amplitude of the  $f_J$  feature depending on the value of  $\beta_c$ . (c) Simulation results for different values of ratio r. When r becomes small, the amplitude ratio in high frequency is suppressed much lower than r.

for large  $f_J$  as illustrated in Fig. 6(c). When r is less than 0.1, the ratio  $A_{4\pi}/A_{2\pi}$  is much smaller than r. This indicates that  $A_{4\pi}/A_{2\pi}$  is further reduced for small r. Though our calculations elucidate some features of Josephson emission, there may be other mechanisms such as Joule heating and quasiparticle poisoning of the  $4\pi$  periodic states [18], which are not captured in the RCSJ model used here.

We can assume that due to the high junction capacitance and possible resulting sizable  $\beta_c$ , the crossover regime between the purely  $4\pi$  periodic and mixed dynamics is inaccessible. Therefore, we are able to access only the high bias regime in which the amplitude of the  $f_{\rm J}/2$  feature would reflect the relative contribution of the  $4\pi$  periodic component in the current phase relationship. Assuming the minimum of a single channel with perfect transmission due to a Majorana mode and a proximity gap of  $\Delta' = 180 \,\mu\text{eV}$  at  $V_g = 80 \,\text{V}$ , we predict  $i_{4\pi} \sim e\Delta'/\hbar \sim 44 \,\text{nA}$  [53]. We estimate  $I_{\text{sw}} = 672 \,\text{nA}$ so that the ratio r is estimated as 0.07. We expect a much more than 14 times weaker emission feature at  $f_{\rm J}/2$  compared with  $f_{\rm I}$  for the high-frequency regime considering the results of Fig. 6. Considering our results, we determine that the noise level is enough to hide the emission amplitude  $A_{4\pi}$ . This is probably due to the large capacitance, which makes all the signal including the  $4\pi$  periodic emission weaker than the noise level. So far, we have only discussed the Josephson emission. However, in the Shapiro step measurement and the Josephson emission measurement, similar conditions are necessary for observation of the  $4\pi$  periodic component [52].

# IV. CONCLUSION

We fabricated gate-tunable JJs on a molecular beam epitaxy grown  $(Bi_{1-x}Sb_x)_2Te_3$  topological insulator. The supercurrent and normal resistance were controlled by a back-gate voltage demonstrating ambipolar transport. The  $I_{sw}R_n$  product

was also gate-voltage-dependent and exhibits a pronounced dip feature near the charge neutral point. This  $I_{sw}R_n$  behavior can be ascribed to the specular Andreev reflection at the boundaries of electron-hole puddles. Finally, by using gate-tunable JJs, we carried out measurement of the ac Josephson effect. By radiating the JJs with microwaves, we observed a conventional pattern of Shapiro steps. We also observed the signature of conventional Josephson emission.

From our results and the support of simulation, it is most probable that small r and large parallel capacitance are the reasons why we are unable to observe the fractional ac Josephson effect. This indicates that  $SrTiO_3$  may be a poor substrate choice for studying the fractional ac Josephson effect due to the high parallel capacitance. The dielectric constant of  $SrTiO_3$  at low temperature is  $\simeq 20\,000$ , and the thickness of  $SrTiO_3$  used in our experiment is  $0.5\,\mathrm{mm}$ . With the same device design, the  $SrTiO_3$  substrate is equivalent to a heavily doped Si substrate covered with 100-nm-thick  $SiO_2$ . This implies that the parallel capacitance does not become remarkably smaller as far as substrates with the back-gate structure are used. Thus we suspect that such substrates are not suitable for observing a missing step.

#### **ACKNOWLEDGMENTS**

This work was partially supported by a JSPS Grantin-Aid for Scientific Research (B) (Grants No. 18H01813 and No. 19H02548), a JSPS Grant-in-Aid for Scientific Research (S) (Grants No. JP26220710 and No. 19H05610), JST CREST (Grant No. JPMJCR15N2), JST PREST (Grant No. JPMJPR18L8), the JSPS Program for Leading Graduate Schools (MERIT) from JSPS, JSPS Research Fellowship for Young Scientists (Grants No. JP18J14172 and No. JP19J13867), NSF-CAREER award (DMR-1847811), and the Gordon and Betty Moore Foundation's EPiQS Initiative (Grant GBMF9063) to C.-Z.C.

- [1] E. Majorana, Nuovo Cimento 14, 171 (1937).
- [2] A. Y. Kitaev, Phys. Usp. 44, 131 (2001).
- [3] A. Y. Kitaev, Ann. Phys. **303**, 2 (2003).
- [4] D. A. Ivanov, Phys. Rev. Lett. 86, 268 (2001).
- [5] C. Nayak, S. H. Simon, A. Stern, M. Freedman, and S. Das Sarma, Rev. Mod. Phys. 80, 1083 (2008).
- [6] R. M. Lutchyn, J. D. Sau, and S. Das Sarma, Phys. Rev. Lett. 105, 077001 (2010).
- [7] Y. Oreg, G. Refael, and F. von Oppen, Phys. Rev. Lett. 105, 177002 (2010).
- [8] L. Fu and C. L. Kane, Phys. Rev. Lett. 100, 096407 (2008).
- [9] L. Fu and C. L. Kane, Phys. Rev. B 79, 161408(R) (2009).
- [10] V. Mourik, K. Zuo, S. M. Frolov, S. R. Plissard, E. P. A. M. Bakkers, and L. P. Kouwenhoven, Science 336, 1003 (2012).
- [11] A. Das, Y. Ronen, Y. Most, Y. Oreg, M. Heiblum, and H. Shtrikman, Nat. Phys. 8, 887 (2012).
- [12] M. T. Deng, C. L. Yu, G. Y. Huang, M. Larsson, P. Caroff, and H. Q. Xu, Nano Lett. 12, 6414 (2012).
- [13] S. M. Albrecht, A. P. Higginbotham, M. Madsen, F. Kuemmeth, T. S. Jespersen, J. Nygård, P. Krogstrup, and C. M. Marcus, Nature (London) 531, 206 (2016).

- [14] L. P. Rokhinson, X. Liu, and J. K. Furdyna, Nat. Phys. 8, 795 (2012).
- [15] J. Wiedenmann, E. Bocquillon, R. S. Deacon, S. Hartinger, O. Herrmann, T. M. Klapwijk, L. Maier, C. Ames, C. Brüne, C. Gould *et al.*, Nat. Commun. 7, 10303 (2016).
- [16] E. Bocquillon, R. S. Deacon, J. Wiedenmann, P. Leubner, T. M. Klapwijk, C. Brüne, K. Ishibashi, H. Buhmann, and L. W. Molenkamp, Nat. Nanotechnol. 12, 137 (2017).
- [17] R. S. Deacon, J. Wiedenmann, E. Bocquillon, F. Domínguez, T. M. Klapwijk, P. Leubner, C. Brüne, E. M. Hankiewicz, S. Tarucha, K. Ishibashi, H. Buhmann, and L. W. Molenkamp, Phys. Rev. X 7, 021011 (2017).
- [18] K. Le Calvez, L. Veyrat, F. Gay, P. Plaindoux, C. B. Winkelmann, H. Courtois, and B. Sacépé, Commun. Phys. 2, 4 (2019).
- [19] R. Yano, M. Koyanagi, H. Kashiwaya, K. Tsumura, H. T. Hirose, T. Sasagawa, Y. Asano, and S. Kashiwaya, J. Phys. Soc. Jpn. 89, 034702 (2020).
- [20] P. Schüffelgen, D. Rosenbach, C. Li, T. W. Schmitt, M. Schleenvoigt, A. R. Jalil, S. Schmitt, J. Kölzer, M. Wang, B. Bennemann *et al.*, Nat. Nanotechnol. 14, 825 (2019).

- [21] D. Laroche, D. Bouman, D. J. van Woerkom, A. Proutski, C. Murthy, D. I. Pikulin, C. Nayak, R. J. J. van Gulik, J. Nygård, P. Krogstrup, L. P. Kouwenhoven, and A. Geresdi, Nat. Commun. 10, 245 (2019).
- [22] S. Nadj-Perge, I. K. Drozdov, J. Li, H. Chen, S. Jeon, J. Seo, A. H. MacDonald, B. A. Bernevig, and A. Yazdani, Science 346, 602 (2014).
- [23] G. C. Ménard, S. Guissart, C. Brun, R. T. Leriche, M. Trif, F. Debontridder, D. Demaille, D. Roditchev, P. Simon, and T. Cren, Nat. Commun. 8, 2040 (2017).
- [24] C. Li, J. C. de Boer, B. de Ronde, S. V. Ramankutty, E. van Heumen, Y. Huang, A. de Visser, A. A. Golubov, M. S. Golden, and A. Brinkman, Nat. Mater. 17, 875 (2018).
- [25] A.-Q. Wang, C.-Z. Li, C. Li, Z.-M. Liao, A. Brinkman, and D.-P. Yu, Phys. Rev. Lett. 121, 237701 (2018).
- [26] A. R. Akhmerov, J. Nilsson, and C. W. J. Beenakker, Phys. Rev. Lett. 102, 216404 (2009).
- [27] S. Park and P. Recher, Phys. Rev. Lett. 115, 246403 (2015).
- [28] S. Park, H.-S. Sim, and P. Recher, arXiv:1812.09573.
- [29] J. Zhang, C.-Z. Chang, Z. Zhang, J. Wen, X. Feng, K. Li, M. Liu, K. He, L. Wang, X. Chen *et al.*, Nat. Commun. 2, 574 (2011).
- [30] D.-X. Qu, Y. S. Hor, J. Xiong, R. J. Cava, and N. P. Ong, Science 329, 821 (2010).
- [31] R. Yoshimi, A. Tsukazaki, Y. Kozuka, J. Falson, K. S. Takahashi, J. G. Checkelsky, N. Nagaosa, M. Kawasaki, and Y. Tokura, Nat. Commun. 6, 6627 (2015).
- [32] S. Ghatak, O. Breunig, F. Yang, Z. Wang, A. A. Taskin, and Y. Ando, Nano Lett. 18, 5124 (2018).
- [33] H. J. Suominen, J. Danon, M. Kjaergaard, K. Flensberg, J. Shabani, C. J. Palmstrøm, F. Nichele, and C. M. Marcus, Phys. Rev. B 95, 035307 (2017).
- [34] J. Gu, W. Cha, K. Gamo, and S. Namba, J. Appl. Phys. 50, 6437 (1979).
- [35] B. Sacépé, J. B. Oostinga, J. Li, A. Ubaldini, N. J. G. Couto, E. Giannini, and A. F. Morpurgo, Nat. Commun. 2, 575 (2011).
- [36] D. Jeong, J.-H. Choi, G.-H. Lee, S. Jo, Y.-J. Doh, and H.-J. Lee, Phys. Rev. B 83, 094503 (2011).

- [37] F. Miao, W. Bao, H. Zhang, and C. N. Lau, Solid State Commun. 149, 1046 (2009).
- [38] H. B. Heersche, P. Jarillo-Herrero, J. B. Oostinga, L. M. K. Vandersypen, and A. F. Morpurgo, Nature (London) 446, 56 (2007).
- [39] X. Du, I. Skachko, and E. Y. Andrei, Phys. Rev. B 77, 184507 (2008).
- [40] J.-H. Choi, G.-H. Lee, S. Park, D. Jeong, J.-O. Lee, H.-S. Sim, Y.-J. Doh, and H.-J. Lee, Nat. Commun. 4, 2525 (2013).
- [41] E. H. Hwang, S. Adam, and S. Das Sarma, Phys. Rev. Lett. 98, 186806 (2007).
- [42] V. V. Cheianov, V. I. Falko, B. L. Altshuler, and I. L. Aleiner, Phys. Rev. Lett. 99, 176801 (2007).
- [43] J. Martin, N. Akerman, G. Ulbricht, T. Lohmann, J. H. Smet, K. Von Klitzing, and A. Yacoby, Nat. Phys. 4, 144 (2008).
- [44] Y. Zhang, V. W. Brar, C. Girit, A. Zettl, and M. F. Crommie, Nat. Phys. 5, 722 (2009).
- [45] K. Komatsu, C. Li, S. Autier-Laurent, H. Bouchiat, and S. Guéron, Phys. Rev. B 86, 115412 (2012).
- [46] C. W. J. Beenakker, Phys. Rev. Lett. 97, 067007 (2006).
- [47] H. Beidenkopf, P. Roushan, J. Seo, L. Gorman, I. Drozdov, Y. S. Hor, R. J. Cava, and A. Yazdani, Nat. Phys. 7, 939 (2011).
- [48] L. Majidi and R. Asgari, Phys. Rev. B 93, 195404 (2016).
- [49] See Supplemental Material at http://link.aps.org/supplemental/ 10.1103/PhysRevB.101.115410 for additional experimental data of sample A.
- [50] F. Dominguez, F. Hassler, and G. Platero, Phys. Rev. B **86**, 140503(R) (2012).
- [51] J. Picó-Cortés, F. Domínguez, and G. Platero, Phys. Rev. B 96, 125438 (2017).
- [52] F. Domínguez, O. Kashuba, E. Bocquillon, J. Wiedenmann, R. S. Deacon, T. M. Klapwijk, G. Platero, L. W. Molenkamp, B. Trauzettel, and E. M. Hankiewicz, Phys. Rev. B 95, 195430 (2017).
- [53] C. W. J. Beenakker and H. v. Houten, Phys. Rev. Lett. 66, 3056 (1991).